COMPARISON OF MAPPING TREES ON FARMLANDS USING MARKOV RANDOM FIELD SUPER-RESOLUTION MAPPING AND MAXIMUM LIKELIHOOD CLASSIFIER

FRANZ ALEX GAISIE-ESSILFIE

May 2013

Supervisors:
Dr. Y.A. Hussin
Dr. E.M. Osei Jnr
V.N.A. Asare

COMPARISON OF MAPPING TREES ON FARMLANDS USING MARKOV RANDOM FIELD SUPER-RESOLUTION MAPPING AND MAXIMUM LIKELIHOOD CLASSIFIER

FRANZ ALEX GAISIE-ESSILFIE

Enschede, The Netherlands, May 2013

Thesis submitted to the Faculty of Geo-Information Science and Earth Observation of the University of Twente and the Faculty of Renewable Natural Resources of the Kwame Nkrumah University of Science & Technology in partial fulfilment of the requirements for the degree of Master of Science in Geo-information Science and Earth Observation.

Specialisation: Natural Resource Management

SUPERVISORS:
Dr. Y.A. Hussin
Dr. E.M. Osei Jnr
V.N.A. Asare

THESIS ASSESSMENT BOARD:
Dr. ir. C.A.J.M. (Kees) de Bie (Chair) ITC, The Netherlands
Dr. B. Kumi Boateng (External Examiner) UMAT, Ghana
Dr. B. E. K. Prah (Internal Examiner) KNUST, Ghana

DISCLAIMER

This document describes work undertaken as part of a programme of study at the Faculty of Geo-Information Science and Earth Observation of the University of Twente and the Faculty of Renewable Natural Resources of the Kwame Nkrumah University of Science & Technology. All views and opinions expressed therein remain the sole responsibility of the author, and do not necessarily represent those of either Faculty.

ABSTRACT

Mapping trees is of prime importance due to their notable ability to absorb carbon dioxide from the atmosphere and store it away for extended periods. In view of this, there have been a number of efforts aimed at maintaining and improving tree stands, notable among them is the REDD+ programme. For such programmes to be effective, there is the need to monitor the rate of increase or loss of forest cover. This is traditionally done by forest inventory, a slow and rather costly process. With the recent advancements in satellite imaging, it is becoming increasingly possible to map features on the ground using remotely sensed data captured by imaging satellites in orbit around the Earth. Due to limitations of small image extent, data availability and in a number of cases, cost, it is not practical to use high resolution satellite images to map trees. Consequently, users often resort to coarser medium resolution images. In view of this challenge and the need to extract more and more information from images, there have been a number of techniques, broadly termed super-resolution mapping techniques, developed to map image pixels at a sub-pixel level. This study compared the relative accuracy of mapping using one such technique, Markov Random Field Super-Resolution Mapping (MRF-SRM), with the Maximum Likelihood Classifier (MLC), a pixel-based classification algorithm in mapping trees on farmlands in two tests; image classification accuracy and tree canopy identification accuracy. An ASTER image of a community in the Ejisu-Juabeng district of Ghana was classified using the MRF-SRM and the MLC techniques after which tests were conducted to compare the image classification accuracy and tree canopy identification accuracy using field data as reference. It was observed that the MRF-SRM technique yielded higher image classification accuracy (74.29%) than the MLC (65.71%). The test of the tree canopy identification accuracy yielded 17.96% and 34.88% for the MRF-SRM and MLC techniques respectively. The results obtained indicate that the MRF-SRM technique is more suitable for mapping large areas than MLC. MRF-SRM, however, less suitable for identifying small targets as compared to MLC.

Keywords: Markov Random Field, super resolution mapping, trees, farmlands

Dedicated to Theresa C. Atobra and V. Nana Ama Asare

ACKNOWLEDGEMENT

Absolute gratitude goes to the Almighty God, the giver of life, health and strength whose boundless grace has brought me thus far. I would also like to acknowledge my supervisors, Dr Y.A. Hussin, Dr E.M. Osei Jnr. and V. Nana Ama Asare whose guidance and inputs have contributed to the making of this work. Utmost gratitude goes to Dr. Thomas Groen, whose handling of R statistical language spurred my interest. My sincere appreciation goes to Dr. Valentyn Tolpekin for his patience and willingness to share his knowledge in the implementation of the Markov-Random Field Super Resolution Mapping technique and taking time off his busy schedules to reply to my emails. To Isaac Kwesi Nooni, Louis Addae-Wireko and Dr Bernard Kumi Boateng (UMAT), I express great gratitude for passing your comments on and reviewing this work.

I also would like to extend warm regards to my colleagues, Eric Atta-Kusi, George Asamoah and Lilian Lucy Lartey. We, "The Endurers" have been able to come this far by supporting each other and I hope we will forever keep in touch. In the same vein, I extend regards to Priscilla Anti, Ebenezer K. Badu and Lily Lisa Yevugah for their diverse support.

I thank my family, especially my mother, Theresa C. Atobra, and my sister, Eunice Gaisie-Essilfie, for their prayers and support. My desire to advance up the academic ladder has been an inspiration for you and your desire to catch up to me has been my source of motivation to push the limit. For this, I am especially thankful.

Last, and definitely not least of all, I acknowledge the support of my good friend, Conrad Kyei. We may be far apart but the memories and strong bonds we forged will surely keep us going. It is my prayer that we meet someday soon to show to the world how far two divergent and yet similar minds can go. I'll be waiting for you at the finish line.

TABLE OF CONTENTS

LIST OF TABLES

LIST OF FIGURES

LIST OF ACRONYMS

ASTER	Advanced Spaceborne Thermal Emission and Reflection Radiometer
FAO	Food and Agriculture Organisation
GDP	Gross Domestic Product
GHG	Greenhouse Gas(es)
GPS	Global Positioning System
HCS	Hyperspherical Colour Sharpening
HNN	Hopfield Neural Network
MLC	Maximum Likelihood Classifier
MR	Medium Resolution
MRF	Markov Random Field
NIR	Near Infrared
REDD	Reducing Emissions from Deforestation and Forest Degradation
SRM	Super Resolution Mapping
VHR	Very High Resolution

1 INTRODUCTION

1.1 Background

Mapping trees is an area of high interest due to the variety of benefits derived from them. One of these benefits is their ability to absorb and store carbon dioxide, a major Greenhouse Gas (GHG) and contributor to climate change, from the atmosphere and store them away for many years, acting as very effective carbon sinks. It goes without saying that when trees are cut down, all the carbon stored in their tissues are released back into the atmosphere, as carbon dioxide through combustion or decay.

Trees generally have about 20 percent of their fresh weight as carbon. In addition, the biomass of forests act as carbon sinks. As a result, forests are known to store over one trillion tons of carbon globally, twice as much as the amount of carbon floating in the atmosphere (FAO, 2006). According to FAO estimates, 135 million hectares of forest have been lost from 1990 to 2010 (FAO, 2010).

In recognition of the importance of forests to mitigating the effects of GHG emissions and an effort to reduce deforestation and forest degradation, there has been the emergence of compliance markets for carbon such as Reducing Emissions from Deforestation and Forest Degradation (REDD) based on the Kyoto Protocol (Dumanski, 2004) which aim to provide nations incentives to maintain and improve their forests. The Kyoto Protocol groups countries into two. These are Annex 1 countries which have developed economies that have GHG reduction targets and Annex 2 countries, with developing economies, which do not have reduction targets for the first period (Dumanski, 2004).

Statistics released by FAO indicate that the rate of deforestation is very high in tropical areas (FAO, 2011). Considering that a lot of countries in the tropical areas are in the list of Annex 2 countries, there is a financial incentive in preserving the tropical forests that exist in these countries (Parker, Mitchell, Trivedi, & Mardas, 2009). In addition to reducing the amount of GHG in the atmosphere and providing financial revenue to the countries that have forests, the preservation of trees and forests will provide other benefits such as watershed protection, water flow regulation, nutrient recycling, rainfall generation and disease regulation (Parker et al., 2009).

Estimating tree stocks is traditionally done by field inventory of sections of forests and then extrapolating the measurements for the entire area covered by the forest. With the development of air- and space-borne remote sensing techniques, it has become possible to determine these estimates without having to engage in the resource-intensive process of doing field inventories. One can acquire images of the desired area and then, by applying image processing techniques and some statistical analyses, the tree stocks of the area can be determined.

The main issue with using remotely sensed images for mapping is that there is an inverse relationship between the spatial resolution of an image and its extent; generally, images with large extent have coarse spatial resolution and vice versa. Due to this, mapping using remotely sensed images faces a major question: high resolution or large spatial extent. One reason for using remote sensing techniques is to reduce cost as compared to using traditional methods of mapping or measurement. Therefore, when choosing images for mapping, a compromise is usually made between extent and resolution such that a relatively high level of detail can be obtained for a reasonably large extent.

When the size of an image pixel is larger than a discrete object on the ground, the value of a pixel will be equal to the integrated effect of the objects that lie within the pixel; that is the sum of the product of the area covered by the objects and their respective DN values (Schowengerdt, 2006). These pixels are commonly called mixed pixels (Kasetkasem, Arora, & Varshney, 2005; Schowengerdt, 2006; Tatem, Lewis, Atkinson, & Nixon, 2001). Owing to the prevalence of mixed pixels, there are a number of methods of spectral unmixing (identification and decomposition of mixed pixels into their pure classes) largely based on sub-pixel classification such as fuzzy c-means clustering, linear mixture modelling and artificial neural networks (Kasetkasem et al., 2005).

Spectral unmixing solves the problem of mixed pixels but in doing that, it creates another. The unmixing process produces results which give the proportions of individual classes in each pixel but does not indicate the spatial location of these classes within the pixel. The absence of spatial location can affect the accuracy of image processing (Tong, Zhang, Shan, Xie, & Liu, 2012). In order to address this challenge, techniques generally classified as Super-Resolution Mapping (SRM) have been developed.

1.2 An Overview of Super Resolution Mapping

With several earth observation satellites in orbit around the earth, there has been a vast increase in the range of applications of remotely sensed images obtained from them. The images obtained from these satellites come with varying spatial, spectral, and temporal resolutions and this affects their suitability for various purposes. For example, the 30-metre resolution images of Landsat are very suitable for applications such as land use planning, agricultural assessment and forest assessment (Stewart, n.d.) while the 0.82-metre resolution of IKONOS images are useful for urban planning and assessment as well as photogrammetry (Dial & Grodecki, 2003).

For most mapping purposes, it is desirable to have images with fine spatial resolution which will provide detailed information. In practice, however, such images may be expensive or unavailable. Moreover the high resolution images do not have a large extent (Muad & Foody, 2010). The alternative is to use images with coarser spatial resolution in which case one has to contend with a high proportion of mixed pixels. Mixed pixels in this context refer to pixels which contain more than one class (Muad & Foody, 2010) for

example, small patches of one class within a larger class, one class blending into another or edge pixels of two classes with a distinct boundary (Figure 1.1).

Mixed pixels pose a challenge for land cover classification since their spectral characteristics do not represent any one distinct land cover type. It is therefore necessary to separate the various classes present within the mixed pixels (spectral unmixing). Among the techniques developed for this purpose are linear and nonlinear spectral mixture analysis, fuzzy *c*-means and artificial neural networks (Atkinson, 2008; Tong et al., 2012).

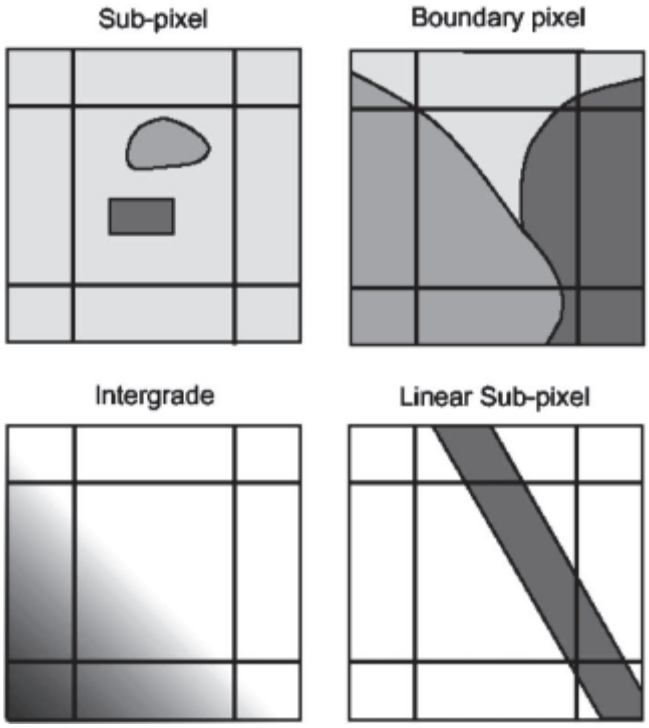

Figure 1.1: Causes of Mixed Pixels (Fisher, 1997)

Though spectral unmixing techniques are able to identify the relative proportions of the various classes within a given mixed pixel, it does not provide information about the location of the various proportions of the classes (Tong et al., 2012). The need to identify the location of the various classes in order to improve the accuracy of image classification led to the development of super resolution mapping techniques.

Super-Resolution Mapping (SRM) refers to the group of image enhancement techniques that take one (Muad & Foody, 2010) or more (Atkinson, 2004) coarse spatial resolution image(s) as input to produce an output at finer spatial scale than the input imagery. There are several ways of achieving this such as Hopfield Neural Network (Tatem et al., 2001), two-point histogram optimisation (Atkinson, 2008), Markov Random Field (Tolpekin, Ardila, & Bijker, 2010) and Variable-Pixel Linear Reconstruction (Merino & Nunez, 2007).

The use of Hopfield Neural Network (HNN) for SRM is described by Tatem et al (2001). In their experiments, they used a Landsat TM image of an agricultural area east of Leicester, UK, as the input.

Validation was done using a 0.5-metre resolution image of the same location. Within the image Tatem et al (2001) focused on a wheat field and a section of airstrip which "provided clearly defined targets with which to evaluate the technique". By applying the HNN to the input images using zoom factors five and seven, an average prediction accuracy of 98.89% was achieved for zoom factor five while zoom factor of seven resulted in a prediction accuracy of 99.72% for the same area. There was no indication, however, of the prediction accuracy of the original Landsat TM image.

Atkinson (2008) presents a paper demonstrating the use of the Two-Point Histogram Optimisation technique. In the paper, Atkinson uses a Boolean model to produce a target output of three classes with dimension 40px × 40px. The target output is coarsened by a zoom factor of 8 to produce an input image of 5px × 5px. Then, using the SRM technique, he increases the resolution of the input by a scale factor of eight. Atkinson tries out two different objectives, point-matching and pattern matching, by optimising and then running the SRM algorithm to each objective. The prediction error for each class is given. However the paper is not conclusive about the suitability of one optimisation over the other or the relative accuracy of the algorithm to other similar ones, aptly stated in the paper as "Further research is required to explore the properties of the algorithm and report on its accuracy relative to other algorithms" (Atkinson, 2008).

The Markov Random Field SRM technique is based on the principle that only neighbouring labels (pixels) have direct interactions with each other (Li, 2009). That is, in a given image, the value of a pixel is influenced only by those pixels that are in close proximity to it.

The technique is demonstrated by Tolpekin et al (2010) and Ardila et al (2011). In both cases, the authors map trees in urban settings. Depending on the location of the tree, the surrounding surface could be pavement, grass or bare soil (Tolpekin et al., 2010). Both papers demonstrate, using a Quickbird image (pixel size 2.4 metres) as input and in-situ verification data, that the Markov Random Field produces an output which has a higher pixel-based accuracy of determining the presence of trees when compared to outputs produced by applying Maximum Likelihood Classifier (MLC) on the same input image (MLC_{kappa} = 0.46, MRF_{kappa} = 0.61 (Tolpekin et al., 2010); MLC_{kappa} = 0.45, MRF_{kappa} = 0.73 (Ardila et al., 2011)).

1.3 Problem Statement

Mapping trees in the environment is of great importance due to the benefits derived from them. In an effort to derive maximal benefits from them, there have been a number of programmes such as REDD (Reduction of Emission from Deforestation and Forest Degradation) aimed at maintaining and possibly, increasing tree carbon stocks. In all such programmes, it is necessary to quickly and reliably determine the amount of forest cover of an area of interest.

The use of forest inventory provides the most reliable measure of forest cover. This approach is however expensive, slow and challenging to produce consistent results. Alternate approaches involve using satellite

images. Using Medium Resolution (MR) satellite image, it is possible to collect data over a large area but the spatial resolution of the images means any form of mapping must rely on development of models and this leads to a high uncertainty. It is possible to use Very High Resolution (VHR) satellite images if one desires to produce results with a low uncertainty. The constraint with using VHR is that they have a small area and the images can be expensive. As a result it is technically impractical to do a wall-to-wall assessment of forest cover and carbon stock estimation due to the high number of images required, especially for large countries (Gibbs, Brown, Niles, & Foley, 2007).

In trying to find a balance between the small areas of VHR images and the low uncertainty of results obtained from MR images, there have been attempts to map trees using different techniques, mostly based on super-resolution and soft-classification. Soft (fuzzy) classification allocates proportions of the various land cover types to the pixels. It however does not indicate the positions of these proportions within the larger pixel (Tong et al., 2012). Super-resolution mapping (SRM) techniques on the other hand use software-based processes to increase the spatial resolution of a coarse resolution image, producing an image with a higher spatial resolution than the original.

Experiments using a variety of SRM techniques have been conducted on diverse data, ranging from simulated data (Atkinson, 2008), through mapping agricultural lands in Europe (Tatem, Lewis, Atkinson, & Nixon, 2003) to mapping trees in urban areas (Ardila et al., 2011). There however has not been any research conducted to determine how well SRM can map trees in tropical areas, especially trees outside forests. It is therefore imperative to conduct research into this area of interest, especially since there is a high rate of deforestation in tropical areas (FAO, 2010).

1.4 Research Objectives

General Objective

The objective of this project is to determine how accurately trees on farmlands can be mapped using Super-Resolution Mapping as compared to using Maximum Likelihood Classifier.

Specific Objectives

In order to meet the general objective, the following specific objectives were formulated:

1. Compare the accuracy of mapping trees on farmlands using Maximum Likelihood Classifier (MLC) and Super-Resolution Mapping (SRM).
2. Determine if the identification of trees on farmlands is affected by the presence of farm crops.

1.4.1 Research Questions

1. Can SRM improve mapping trees on farmlands with reference to MLC?
2. Does the presence of farm crops affect the identification of trees using SRM?

2 MATERIALS AND METHODS

2.1 Study Area

The study was carried out in the Ejisu-Juabeng District, one of the 27 administrative districts in the Ashanti Region of Ghana. It lies within latitude 1.15°N and 1.45°N and longitude 6.15°W and 7.00°W and has an area of 637.2 square kilometres (Ministry of Food & Agriculture, Ghana, 2011) (Figure 2.1).

As is the case with the mid-section of Ghana, rainfall pattern in the district is bimodal with annual rainfall ranging from 1092 to 2344 mm with a mean annual value of about 1874 mm. Rainfall usually occurs from March to July and then from September till November. The mean maximum temperature is about 32°C, occurring in February/March and the mean minimum temperature is about 20°C, occurring in December/January. The mean monthly temperature in the district is approximately 26°C. Relative humidity averages at 85% during the rainy season and 65% during the dry season (Anornu, Kortatsi, & Saeed, 2010; Ministry of Food & Agriculture, Ghana, 2011).

Agriculture is the main economic activity in the district, accounting for 58.55% of the district's GDP (Anornu et al., 2010). About 55.6% of the total employed labour force in the district are into agriculture and the farming intensity is 69.54% (Ministry of Food & Agriculture, Ghana, 2011). The major agricultural production is food crops (e.g. maize, plantain, cassava and cocoyam) and tree crops (e.g. cocoa, oil palm and citrus).

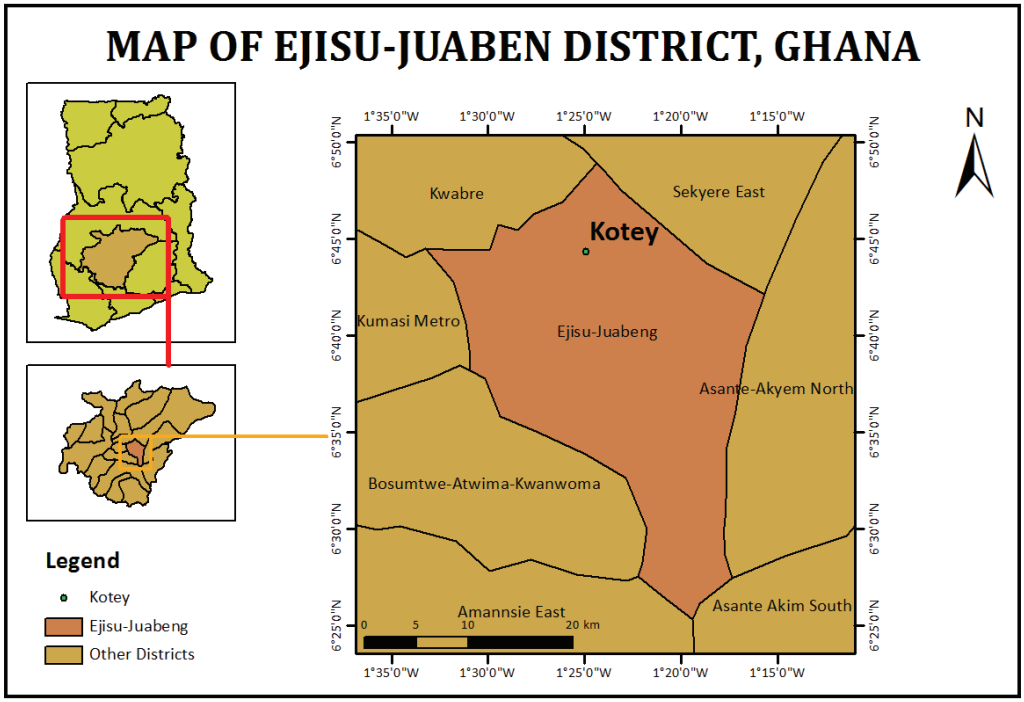

Figure 2.1: Map of Ejisu-Juabeng District, Ghana

2.1.1 Data Collection Site

An initial survey of selected communities in the district revealed that trees are not kept in oil palm plantations. The farmers indicated the shade they cast hampers the growth and productivity of the oil palm. This meant that one is not likely to find many trees in farms in those communities where the major economic activity is growing oil palm. Further inquiries revealed that one is most likely to find trees in cocoa plantations since cocoa does well in shade. These statements were confirmed by a survey of a number of communities in the district.

Based on the information received from the farmers and data obtained from surveys, the Kotey community (6° 44' 22.3764" N, 1° 24' 55.1808" W) of the Ejisu-Juabeng district was chosen for data collection (Figure 2.2).

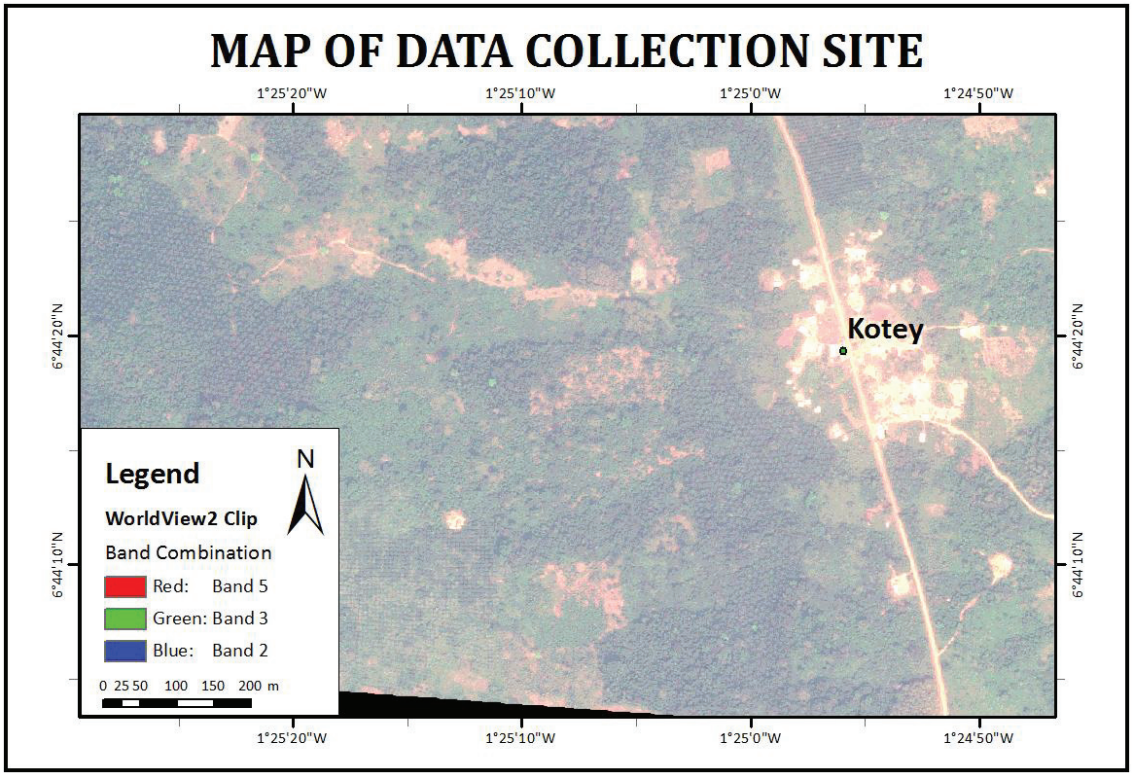

Figure 2.2: Map of Data Collection Site

2.2 Data

2.2.1 Satellite Images

A WorldView-2 satellite image acquired on January 4, 2011 was used for selecting sampling sites in the pre-fieldwork stage. It was also used to augment selection of sampling points for classification of the ASTER

image. An ASTER Image acquired on February 6, 2011 was used in addition to the WorldView-2 image for the study. The ASTER image was classified using the Maximum Likelihood Classifier (MLC) and then the Markov Random Field (MRF) super-resolution mapping technique. The characteristics of the satellite images used for the study are detailed in Table 2.1 and Table 2.2.

Table 2.1: Characteristics of WorldView-2 image used (Satellite Imaging Corporation, n.d.)

Band	Spectral Range (nm)	Spatial Resolution (m)	Dynamic Range
Panchromatic	450 – 800	0.46 (resampled to 0.5)	
Band 1(Coastal)	400 – 450		
Band 2 (Blue)	450 – 510		
Band 3 (Green)	510 – 580		
Band 4 (Yellow)	585 – 625	1.8	11 bits per pixel
Band 5 (Red)	630 – 690		
Band 6 (Red Edge)	705 – 745		
Band 7 (NIR 1)	770 – 895		
Band 8 (NIR 2)	860 – 1040		

Table 2.2: Characteristics of ASTER Image Used (Abrams & Hook, n.d.)

Band No.	Spectral Range (μm)	Spatial Resolution (m)	Quantization Levels
1 (Green)	0.52 – 0.60		
2 (Red)	0.63 – 0.69	15	8 bits
3 (NIR)	0.78 – 0.86		

It was observed however that contrary to the data stated in Table 2.2, the ASTER image had a spatial resolution of 16.980949m × 16.980949m.

Both images used were in the WGS 1984 UTM Zone 30N projection system with the WGS 1984 datum and spheroid.

2.2.2 Shape Files

Shape files of Administrative Regions and Administrative Districts of Ghana were obtained from the Ghana Country at a Glance database for the study. These shape files were used to prepare maps of the study area. They were also used in clipping the ASTER satellite image to the study area.

2.3 Pre-Fieldwork

2.3.1 Satellite Image Processing

2.3.1.1 Pan-Sharpening

Pan-sharpening refers to the group of techniques that increase the spatial resolution of an image by combining lower resolution multispectral pixels with higher resolution panchromatic pixels to produce a high resolution multispectral image. As demonstrated by Padwick et al (2010), the Hyperspherical Colour Sharpening (HCS) algorithm is very suitable for pan-sharpening World View-2 images. ERDAS Imagine 2011 was used to obtain a 0.5-metre resolution World View-2 image from the 8 multispectral bands using the HCS resolution merge pan-sharpening tool.

2.3.1.2 Co-registration

After the pan-sharpening process, the two satellite images used in the study (WorldView-2 and ASTER images) were found to be offset relative to each other by approximately 32 metres in the horizontal direction. To correct this, the ASTER image was co-registered to the WorldView2 image using ArcGIS.

2.3.2 Sample Site Selection

Using the WorldView-2 image of the study area, the study area was broadly classified into two; areas with vegetation cover and those without vegetation cover. Those places marked as having vegetation were then divided into oil palm and others. This separation was done based on visual identification. Oil palm plantations were easily identifiable from the stellate canopy profile and the triangular mesh pattern of the trees.

After separating the oil palm from the other vegetation types, preliminary field survey was carried out to determine whether the non-oil palm vegetation cover could be broken down into distinct subcategories. This was found to be possible and resulted in three more categories (citrus trees, cocoa trees and mixed farms/fallow) being created.

The mixed farms could not be readily separated from the fallow areas because the survey was carried out in October, when annual crops have been harvested and the land is left to fallow till the next growing season. In such cases, the vegetation cover was similar with the exception that land that had been recently cultivated had less vegetation cover than those that had been left for a year or longer (Figure 2.3). In most cases, the crops that were previously grown on the land could not be reliably identified.

After the preliminary survey and categorisation, six classes, namely built-up/bare, citrus trees, oil palm, cocoa trees, mixed farms/fallow and trees were identified. Table 2.3 contains the classes and the major identified features peculiar to the class.

Figure 2.3: Fresh fallow (left) and old fallow (right)

Table 2.3: Description of classes identified

Class	Dominant Feature
Built-up/Bare	Bare soil or buildings
Citrus Trees	Citrus trees
Cocoa Trees	Cocoa trees
Mixed Farms/Fallow	Other annual crops, native vegetation
Oil Palm	Oil palm trees
Trees	Woody perennials not cultivated as a crop

2.3.3 Tree Selection Criteria

Since the classification of the study area would be done on an ASTER image with pixel size of 15m × 15m, it was determined that a candidate tree for recording has an average canopy extent of 12 metres. This minimum requirement was based on the fact that ASTER image, which would be used for the MLC classification and subsequent super-resolution analysis, has a pixel size of 15m × 15m. Assuming, therefore, that the entire canopy of a given tree lies completely within a pixel and the shape of the canopy is elliptical and the major and minor diameters of the canopy are 14m and 10m respectively, the area of the canopy of that tree would be given as follows:

$$A = \pi ab$$
$$= \pi \left(\frac{14\ m}{2}\right)\left(\frac{10\ m}{2}\right)$$
$$= \pi \times 7m \times 5m$$
$$A = 109.95574\ m^2$$

Thus, approximately 50 percent of the pixel would be occupied by the tree's canopy and thus the pixel would be classified as a tree if MLC is used.

$$\frac{109.95574\ m^2}{15\ m^2 \times 15\ m^2} \times 100 = 48.86922\%$$

2.4 Field Data Collection

2.4.1 Tree Canopy Measurement

Following the categorisation of the study area, places marked as cocoa farms were visited. Trees that met the minimum selection criteria described in section 2.3.3 above were located and the minimum and maximum canopy extent was measured. In recording the canopy extents, the two were taken such that they would be mutually perpendicular as shown in Figure 2.4. The locations of these trees were also recorded using a handheld Global Positioning System (GPS) receiver. A total of 57 trees were recorded in this study.

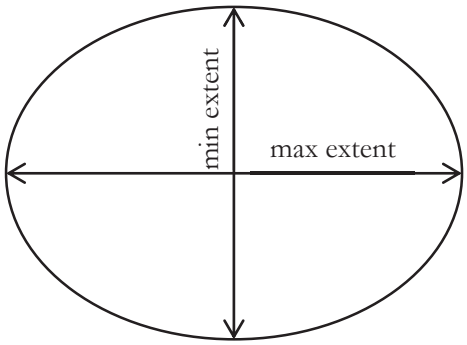

Figure 2.4: Measurement of canopy extent

2.4.2 Sampling for Image Classification

The locations of representative samples of the land cover types identified (see Table 2.3) were recorded using a handheld GPS receiver. The points sampled were taken such that the minimum distance between any two points of the same class was 30 metres. These points would be used later for image classification and accuracy assessment of the classified images.

2.5 Post-Fieldwork Data Processing and Analysis

2.5.1 Delineating Tree Canopies

The coordinates of the trees identified and measured on the field were imported as a point shape file into ArcMap and overlaid on the WorldView-2 image to ease locating and identification of the orientation of the tree canopies. ArcMap was set to display Band 7 of the image rather than a natural colour composite in order for the contrast between the trees and surrounding vegetation (see Figure 2.5). A polygon shape file was then created to hold the delineated trees. The tree canopies identified on the field were then drawn to the polygon shape file using the freehand shape editing tool in ArcMap to match the dimensions measured on the field and the canopy orientation in the image.

(a) (b)

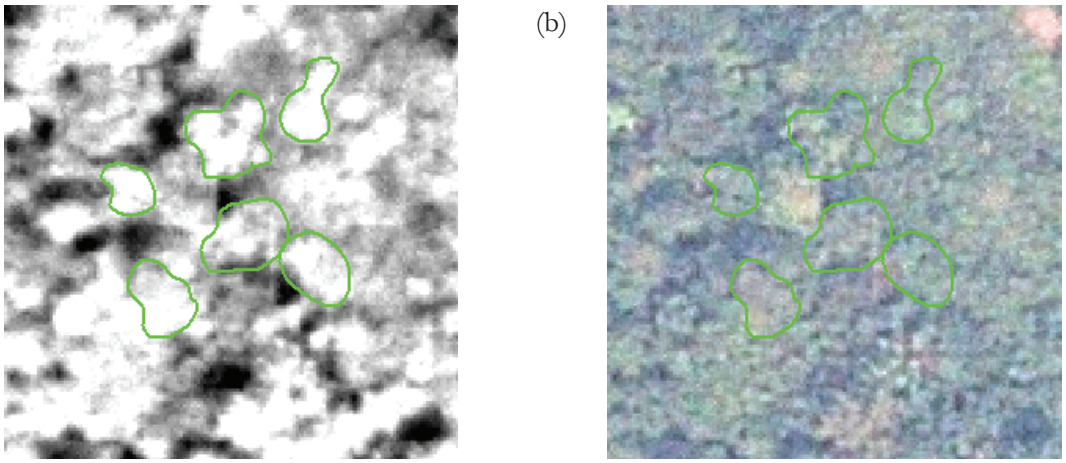

Figure 2.5: Delineating tree canopies with WorldView-2 image
(a) Band 7
(b) Natural Colour Composite (R:5, G: 3, B: 2)

2.5.2 Image Classification and Super Resolution Mapping

With the sample points collected from the field, the ASTER image was classified into the classes stated in Table 2.3 with ERDAS Imagine using the Maximum Likelihood Classifier. The pixel values of the sampled points were also recorded from the unclassified ASTER image using the Identify Tool in ArcMap. These values were then used to calculate means and covariances of the various classes which were saved into text files for performing the MRF-SRM.

After calculating the means and covariances, the text files as well as ASTER image of the study area were loaded into RStudio (*RStudio: Integrated development environment for R*, 2012) running on R v2.15.1 (R Core Team, 2012), where a script for performing the Markov Random Field super-resolution mapping was run on it. The target zoom level of the MRF-SRM was set to 4. This produced an output image with pixel size of 4.2452373m × 4.2452373m from the original resolution of 16.980949m × 16.980949m.

2.5.3 Accuracy Assessment

After the ASTER image had been classified using the Maximum Likelihood Classifier and then the Markov Random Field Super-Resolution Mapping two tests of accuracies were conducted; a test of how accurately the whole image was classified and a test of how accurately trees were identified.

2.5.3.1 Whole Image Classification Accuracy

In this test, a set of validation points, which was a subset of the sample points collected for classification of the images, was used to test the accuracy with which each of the methods correctly identified the land cover type of a given location. Though the two images were of different spatial resolutions, the same validation points were used for the accuracy assessment.

The basis of this decision was that given a mixed pixel with more than one class as in Figure 2.6(a), the entire pixel gets classified as Class A when classified with MLC due to the fact that the dominant class is Class A. This affects the accuracy report because a validation point taken at the location of the pink box and the red box will both be Class A even though the red box is dominated by class B. When the same pixel is run through an SRM with zoom factor 4 as in Figure 2.6(b), then the dominant feature of the location marked by the red box (Class B) gets assigned that pixel.

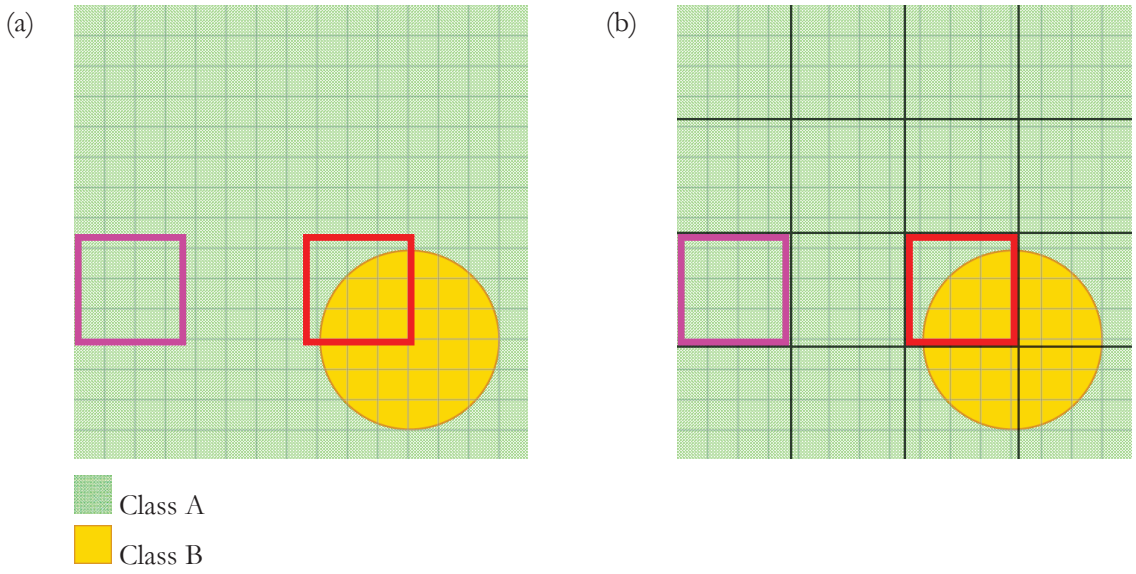

Figure 2.6: Accuracy assessment of mixed pixel
(a) Before SRM
(b) After SRM

The validation points were converted to a point shape file. The Sample tool in ArcMap was then used to sample pixel values from the MLC and MRF-SRM. The DBF file produced by the Sample Tool was then exported to Microsoft Excel and the land cover observed in the field was appended to the table as a new column.

A contingency table each was produced for the MLC results and the MRF-SRM results. From the contingency table, the overall image classification accuracies for both classification techniques were calculated.

2.5.3.2 *Object Identification Accuracy*

This test's objective was to determine the level at which both classification techniques correctly identified tree canopies. In order to do this, a buffer was created around the digitised shape files of tree canopies. The buffer value was set to a quarter of the size of a pixel for each of the images to be assessed (i.e. a 4.25 metre buffer was used for the MLC-classified image and a 1 metre buffer for the MRF-SRM output). This buffering process was necessary because without itthe tree canopies that were smaller than a pixel or straddling two or more pixels were not extracted (Figure 2.7). The Extract by Mask tool in ArcMap was then used to extract the pixels of the image that represent canopies measured on the field.

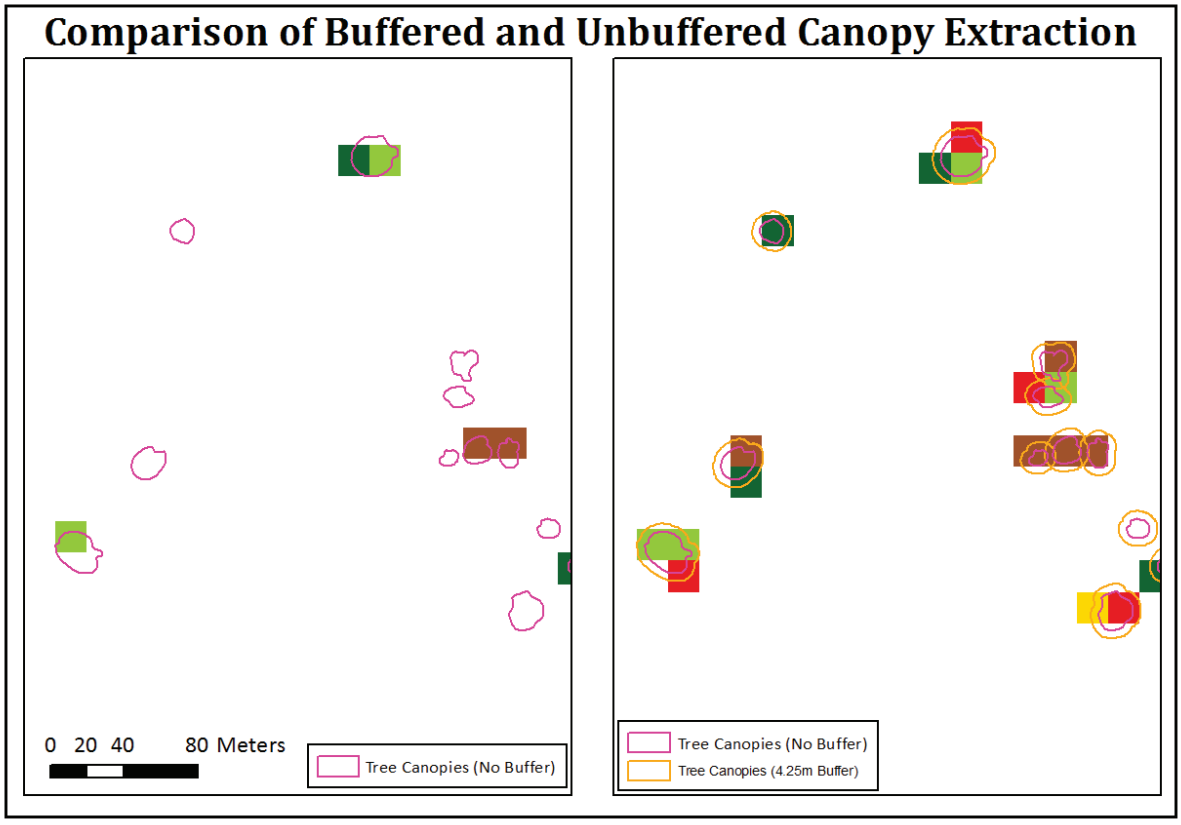

Figure 2.7: Comparison of unbuffered and buffered canopy extraction of MLC Output

After the extraction of the canopy pixels, the Frequency tool of ArcMap was used to count the frequencies of the classes in the extracted pixels. This table represented the number and classes of the classified image that were recorded as tree canopies on the field. By adding an additional column to the frequency table produced by ArcMap and calculating the product of the frequencies and the pixel size, the area covered by the various classes was obtained.

2.5.4 Test of Hypothesis

2.5.4.1 Whole Image Classification

A t-test was performed to determine whether the difference observed in the image classification accuracy obtained using both methods was statistically significant. The data used for accuracy assessment, whose columns were RealValue, MLC and MRF with 70 samples, a bootstrap of 5000 replicates of 50 samples per replicate was performed to produce a normally distributed dataset. The dataset was then imported into the R environment where the `t.test` command of the `stats` package was used to perform a t-test on the sample at 95% confidence interval ($\alpha = 0.05$).

2.5.4.2 Object Identification Accuracy

Since there were a number of canopies in such close proximity that they shared common pixels, this made it impractical to extract the individual canopies and perform a bootstrap on the data to obtain a normally distributed dataset which would then be used as input data for a t-test to determine the statistical significance of the observed difference. A chi-square test was therefore performed on the results using a confusion matrix produced from the canopy identification accuracy. The chi-square test was performed, rather than the t-test, because the chi-square test is more suitable to determine the association between two variables when the entire population is unavailable (Weiss, 2012). The chi-square test was performed in the R environment using the `prop.test` command of the `stats` package at 95% confidence interval ($\alpha = 0.05$)

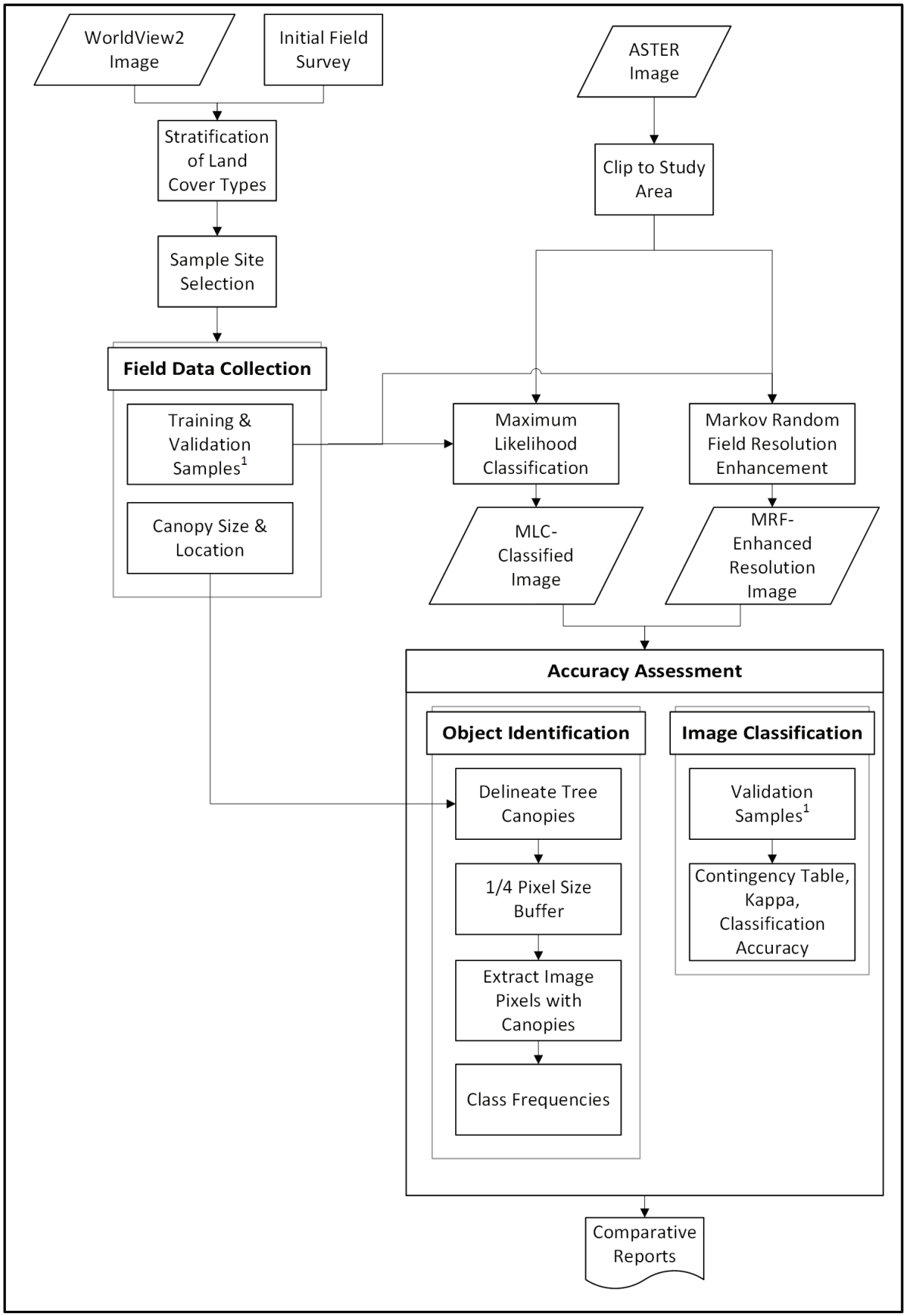

Figure 2.8: Flowchart of Methods

CHAPTER THREE

3 RESULTS

3.1 Tree Canopy Measurements

A total of fifty-seven tree canopies were measured on the field and subsequently located and digitised. The minimum extent of the tree canopies was found to range from 4.8 metres to 20.4 metres while the maximum extent ranged from 6.0 metres to 26.4 metres. The mean canopy extent was also calculated and found to range from 5.4 metres for the tree with smallest canopy extent to 22.4 metres for the tree with the largest canopy extent (Figure 3.1).

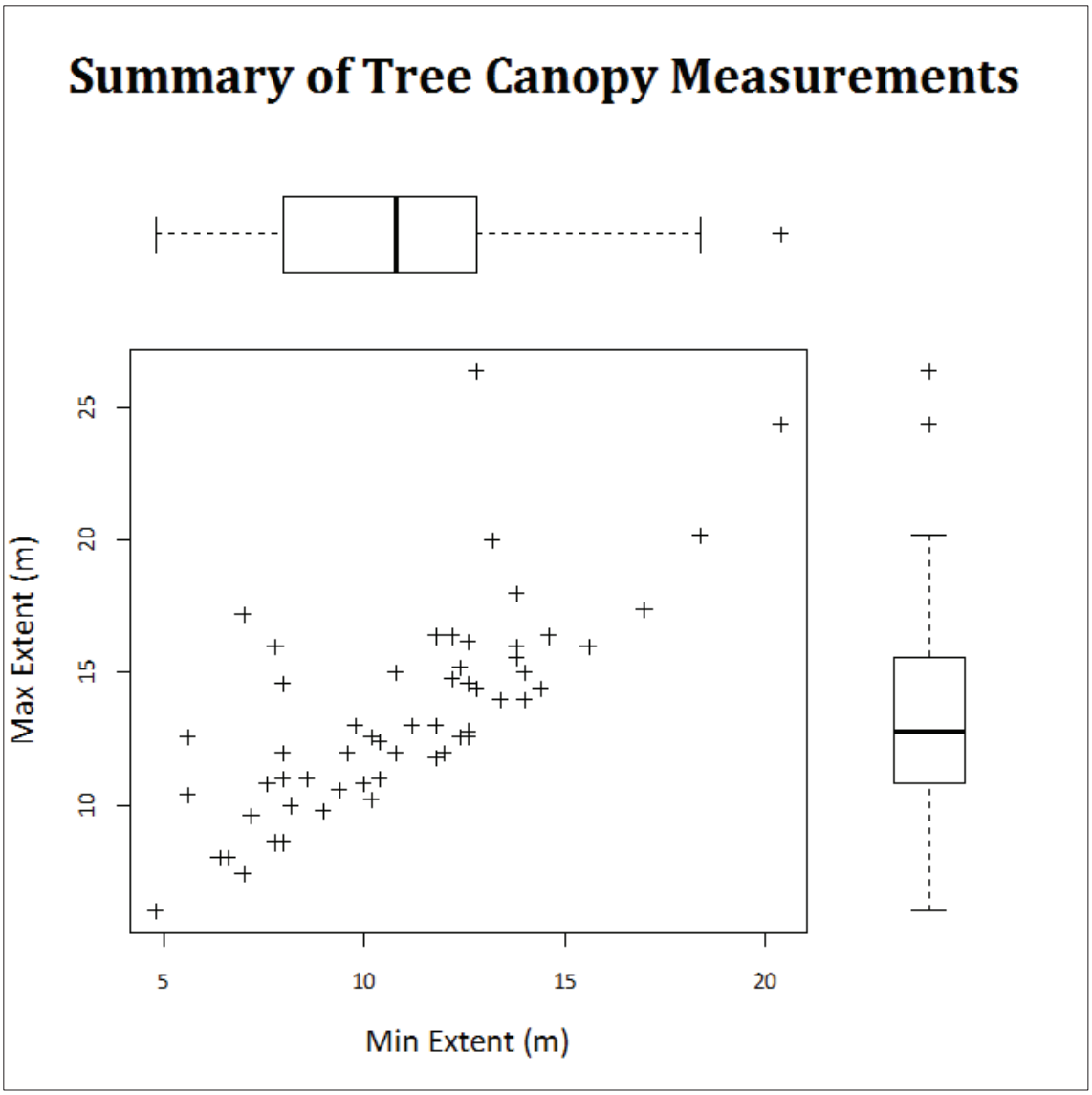

Figure 3.1: Box plot of tree canopy measurement

Based on the measurements, it was found that the tree canopy area ranged from 22.62 square metres to 390.90 square metres. The mean tree canopy area was 121.90 square metres which is approximately 50% of a pixel on the ASTER image (Figure 3.2). This implies therefore, if a tree is located entirely within a pixel, then the pixel corresponding to said tree will be classified as 'Tree'. This is however the ideal case as in reality all the trees may not always be positioned entirely within a pixel.

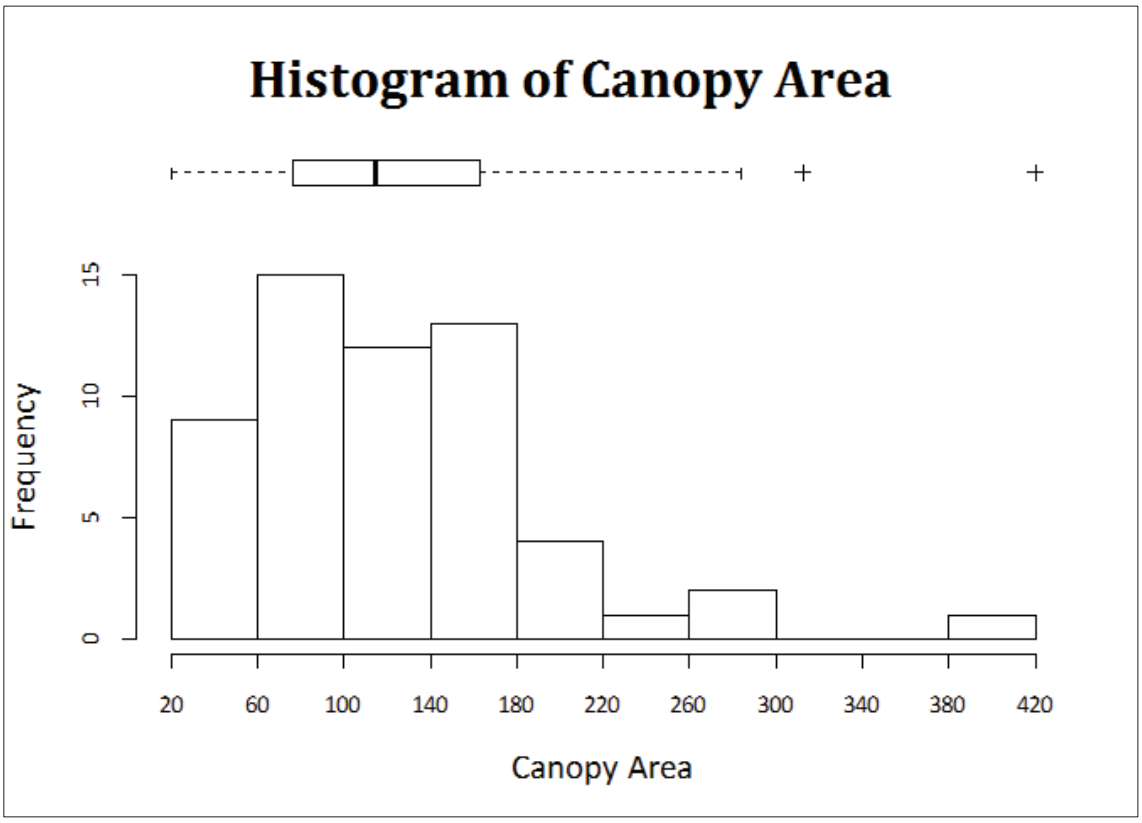

Figure 3.2: Histogram of Canopy Area

3.2 Image Classification

Figure 3.5 shows the Maximum Likelihood Classification output and Figure 3.6, the output of classification using the Markov Random Field Super-Resolution Mapping technique. The pixel size of the MLC output is 16.981m while the MRF-SRM output has a pixel size of 4.245m.

3.3 Accuracy Assessment

As stated in section 2.5.3, there were two types of accuracy assessments performed; accuracy assessment of classification of the whole image and then, the accuracy of tree canopy identification. This is because this project intended to compare the effectiveness of MLC classifier and MRF in mapping trees on farmlands, and the relative canopy identification accuracy of both techniques.

Table 3.2 and Table 3.3 show the contingency tables of the classification accuracy of the whole image using the Maximum Likelihood Classifier and Markov Random Field Super-Resolution Mapper respectively. The classification accuracy achieved using MLC was found to be 65.71% while MRF-SRM achieved an overall accuracy of 74.29%.

Table 3.1 shows the accuracy with which both techniques were able to identify tree canopies that were measured in the field. It is seen that of the 43 pixels that were extracted as trees from the MLC output using the procedure described in section 2.5.3.2, only 15 representing 34.88% were correctly identified. In the case of the MRF output, 67 pixels out of the actual 373 pixels were correctly identified as trees. This represents a 17.96% accuracy in tree canopy identification by the MRF-SRM. From this result, it is seen that the Markov Random Field Super-Resolution Mapping technique has a lower canopy identification rate than the Maximum Likelihood Classifier.

Table 3.1: Canopy Identification Accuracy

	Pixel Count		Area (square metres)	
	MLC	**MRF**	**MLC**	**MRF**
Built-Up/Bare	1	5	288.3526	90.1102
Citrus Trees	1	19	288.3526	342.4187
Cocoa Trees	9	101	2595.174	1820.226
Fallow/ Mixed Farms	8	57	2306.821	1027.256
Oil Palm	9	124	2595.174	2234.733
Tree	15	67	4325.289	1207.477
Total	**43**	**373**	**12399.16**	**6722.221**
	34.88%	**17.96%**	**34.88%**	**17.96%**

3.4 Test of Hypothesis

3.4.1 Whole Image Classification

The following hypothesis was tested to determine the statistical significance of the difference between the image classification accuracy results obtained using the MLC and MRF-SRM:

H_0: There is no significant difference between the results obtained using either methods.

H_1: The result obtained using MRF-SRM is significantly higher than the result obtained using MLC.

A t-test done in R using the bootstrapped data produced from the accuracy assessment dataset as described in 2.5.4.1. At 95% confidence interval ($\alpha = 0.05$) the p-value was 1. This indicates that the difference between the difference in image classification accuracy observed between the MLC and MRF-SRM is statistically significant at α level 0.05.

```
> t.test(repl$MLC, repl$MRF, alternative="g")

        Welch Two Sample t-test

data:  repl$MLC and repl$MRF
t = -127.625, df = 9948.972, p-value = 1
alternative hypothesis: true difference in means is greater than 0
95 percent confidence interval:
 -0.08896815         Inf
sample estimates:
mean of x mean of y
 0.651696  0.739532
```

Figure 3.3: Output from R console of t-test result

3.4.2 Object Identification

The following hypothesis was tested to determine the significance of the difference between the results obtained from the object identification test using the MLC and MRF-SRM techniques:

H_0: There is no significant difference between the object identification accuracy using either method.

H_1: The result obtained using MRF-SRM is significantly different from the object identification accuracy obtained using MLC.

Using the `prop.test` function in R, the p-value was found to be 0.01 at 95% confidence interval. This implied that the null hypothesis is invalid and must be rejected.

```
> prop.test(c(15, 67), c(43, 373))

        2-sample test for equality of proportions with continuity correction

data:  c(15, 67) out of c(43, 373)
X-squared = 5.9473, df = 1, p-value = 0.01474
alternative hypothesis: two.sided
95 percent confidence interval:
 0.008560904 0.329864185
sample estimates:
   prop 1    prop 2
0.3488372 0.1796247
```

Figure 3.4: Output from R console of chi-square test result

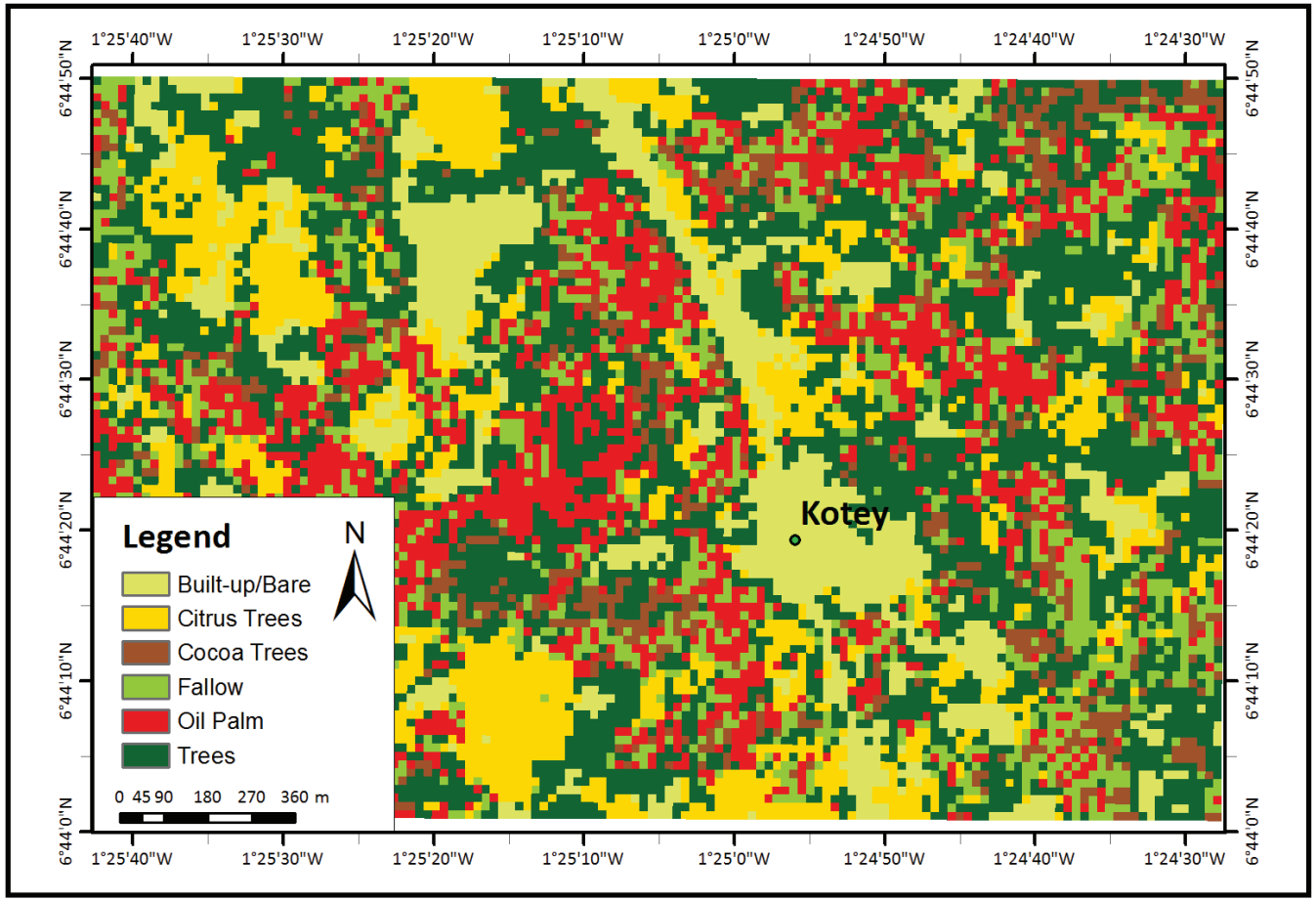

Figure 3.5: Output of Maximum Likelihood Classifier

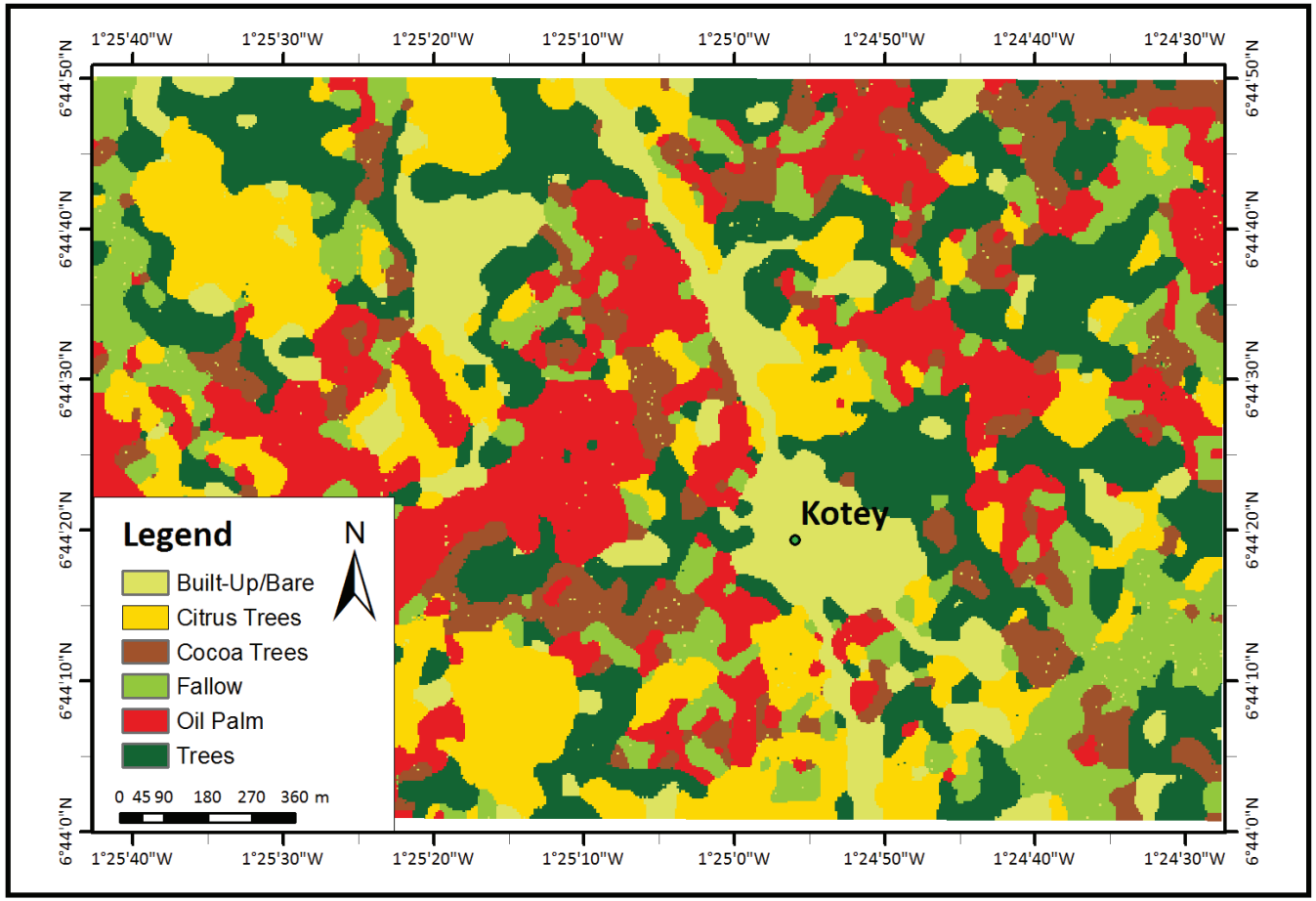

Figure 3.6: Output of Markov Random Field Super-Resolution Mapper

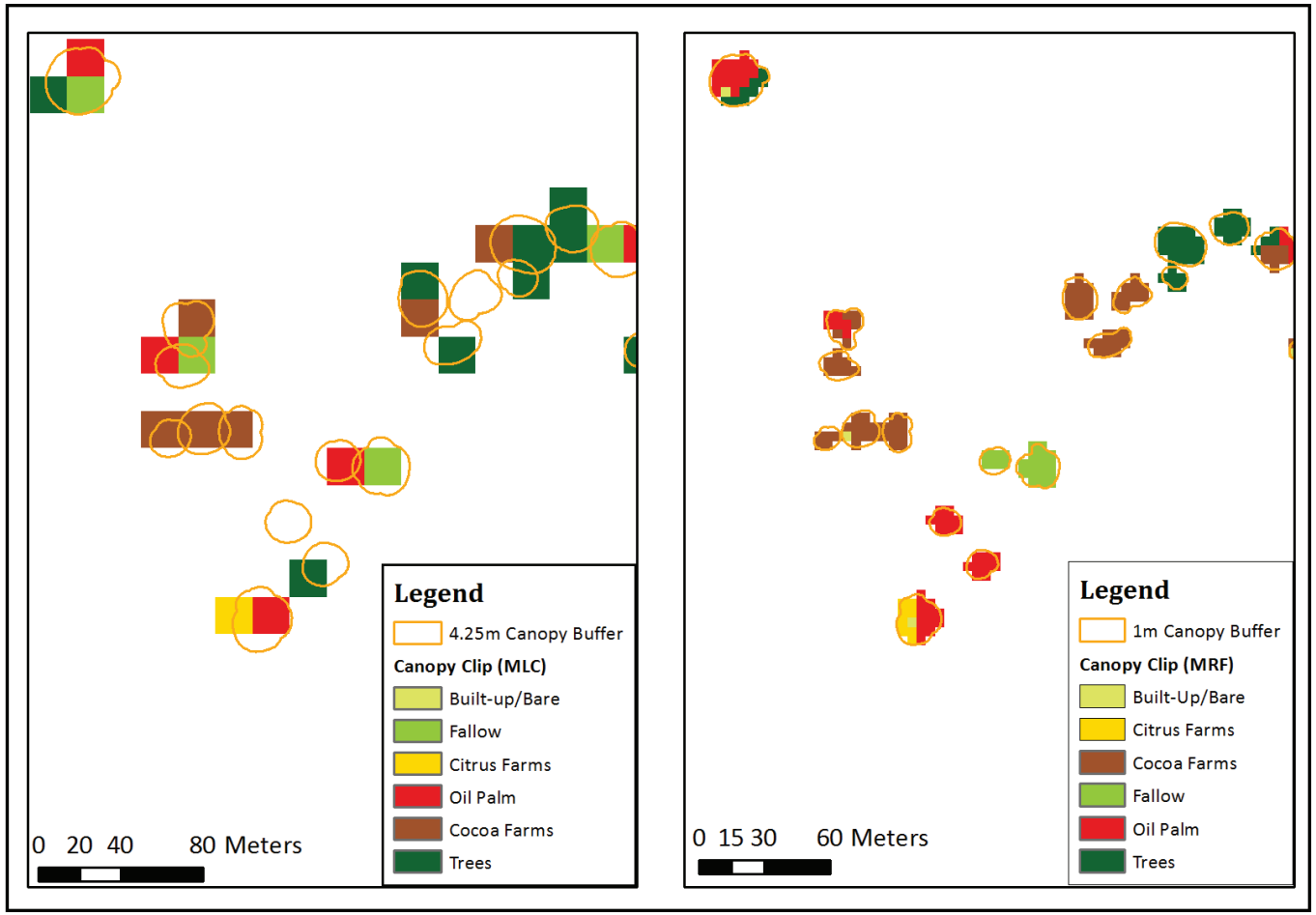

Figure 3.7: Comparison of Canopy Extraction of the two Mapping Techniques

Table 3.2: Contingency Table of Image Classification with Maximum Likelihood Classifier

		Maximum Likelihood Classifier								
	Class	**Built-Up/Bare**	**Citrus Trees**	**Cocoa Trees**	**Fallow/ Mixed Farms**	**Oil Palm**	**Trees**	**Total**	**Error of Omission**	**Producer Accuracy**
Ground Data	**Built-Up/Bare**	6	1	0	0	0	1	8	25.00%	75.00%
	Citrus Trees	0	6	0	0	0	0	6	0.00%	100.00%
	Cocoa Trees	0	0	4	0	0	0	4	0.00%	100.00%
	Fallow/ Mixed Farms	0	0	1	4	0	2	7	42.86%	57.14%
	Oil Palm	0	2	0	1	12	1	16	25.00%	75.00%
	Trees	1	2	0	11	1	14	29	51.72%	48.28%
	Total	7	11	5	16	13	18	70		
	Error of Commission	14.29%	45.45%	20.00%	75.00%	7.69%	22.22%			
	User Accuracy	85.71%	54.55%	80.00%	25.00%	92.31%	77.78%			

Overall Accuracy: 65.71%

Cohen's Kappa Statistic: 0.571

Table 3.3: Contingency Table of Image Classification with Markov Random Field Super-Resolution Mapper

		Markov Random Field Super-Resolution Mapper								
	Class	**Built-Up/Bare**	**Citrus Trees**	**Cocoa Trees**	**Fallow/ Mixed Farms**	**Oil Palm**	**Trees**	**Total**	**Error of Omission**	**Producer Accuracy**
Ground Data	**Built-Up/Bare**	6	0	0	0	0	0	6	0.00%	100.00%
	Citrus Trees	0	10	0	2	0	1	13	23.08%	76.92%
	Cocoa Trees	0	0	5	4	0	0	9	44.44%	55.56%
	Fallow/ Mixed Farms	0	0	0	6	2	1	9	33.33%	66.67%
	Oil Palm	0	1	0	2	11	2	16	31.25%	68.75%
	Trees	1	0	0	2	0	14	17	17.65%	82.35%
	Total	7	11	5	16	13	18	70		
	Error of Commission	14.29%	9.09%	0.00%	62.50%	15.38%	22.22%			
	User Accuracy	85.71%	90.91%	100.00%	37.50%	84.62%	77.78%			

Overall Accuracy: 74.29%

Cohen's Kappa Statistic: 0.686

The Cohen's Kappa statistic calculated from the two contingency tables gave 0.571 and 0.686 for MLC and MRF-SRM respectively. These values indicate that 57.01% of the pixels classified using MLC agreed with the field data collected. MRF-SRM on the other hand had a higher agreement rate of 68.59%. Based on these two accuracy assessment statistic (percent agreement and kappa statistic), it can be seen that with the same inputs, MRF-SRM produces outputs with a higher accuracy than using MLC.

Due to the difference in resolution of the output images, the area extracted by the delineated tree canopies were different. The MLC output, with a 16.98 metre resolution, had a smaller number of pixels and, by extension, area of extracted pixels than the MRF-SRM output which had a pixel size of 4.25 metre resolution.

CHAPTER FOUR

4 DISCUSSION

4.1 Image Scaling

Scale is the ratio between two sizes, usually the size of a representation (e.g. a map) and the size of the actual object in reality (e.g. actual distance on the ground) (Atkinson, 2004). The effect of scale is easily observed in raster images, where it is manifested as the spatial resolution of a given image. It must be noted, however, that scale and spatial resolution are not the same.

Once acquired, the spatial resolution of a raster image cannot be altered without modifying the image's pixel values. Changing from a fine spatial resolution to a coarse spatial resolution or reducing detail is called upscaling and changing from a coarse spatial resolution to fine spatial resolution or increasing detail is called downscaling (see Figure 4.1).

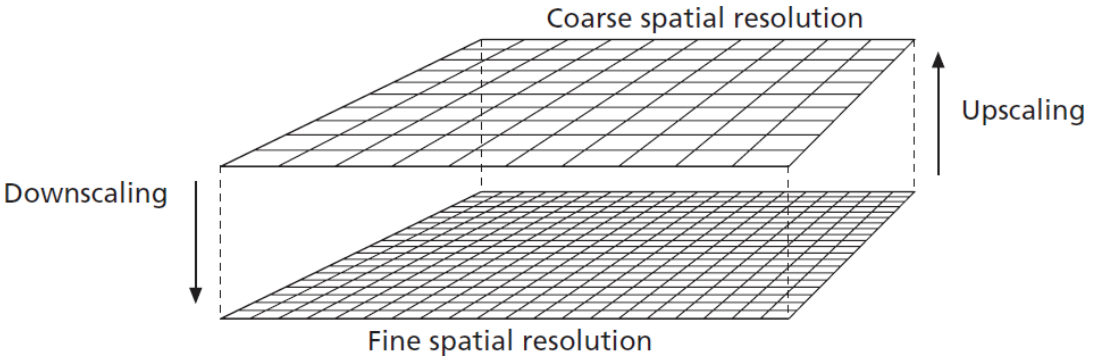

Figure 4.1: Two different spatial resolutions illustrating upscaling and downscaling (Atkinson, 2004)

Upscaling an image is a relatively easy operation that involves aggregation of the pixels of the input image using functions such as mean and simple majority. Downscaling, on the other hand, is fairly more complicated as it attempts to do the seemingly impossible task of extracting more information than what is available. This consequently involves more advanced sub-pixel mapping techniques such as Hopfield Neural Network (Tatem et al., 2001), two-point histogram optimisation (Atkinson, 2008), Markov Random Field (Tolpekin et al., 2010) among others.

This research followed along a pattern similar to Ardila et al. (2011) in identifying urban trees in Very High Resolution (VHR) satellite images using Markov Random Field Super-resolution Mapping. The difference in this research is that the research aimed at identifying trees on farmlands and it used a Medium Resolution (MR) image, rather than a VHR image.

4.2 Image Classification Accuracy

Similar to the results achieved by Ardila et al. (2011), the image classification accuracy of the MRF-SRM technique was almost 10% better than using MLC, a pixel-based classification technique (Table 3.2 and Table 3.3). A t-test of the difference between the two techniques revealed that this improvement in image classification accuracy is statistically significant at a 95% confidence interval ($\alpha = 0.05$). This marked increase in classification accuracy is likely due to the fact that the MRF-SRM technique increases the homogeneity and isotropy (Li, 2009).

In other words, the MRF-SRM technique reduces the chance of finding a pixel of class A whose neighbourhood is made up almost entirely of another class, say, B. As a result the output appears smoother as against the salt-and-pepper output produced by pixel-based classification. This property of the Markov Random Field technique makes it very suitable for reliably identifying large expanse features such as those that are approximately 7×7 pixels or larger.

4.3 Object Identification Accuracy

Contrary to expectations based on the image classification results, the smoothing effect of the Markov Random Field technique made it poor at identifying isolated features or classes. This was observed in the object identification part of the research where the accuracy of mapping trees on farms was performed. In the object identification test it was observed that the MRF-SRM output performed markedly poorer than the MLC output, correctly identifying only 17.96% of the tree canopies delineated as against 34.88% obtained using the Maximum Likelihood Classifier (Table 3.3).

A possible reason for the relatively low accuracies of object identification of both techniques could be the size of the objects (tree canopies) in relation to the input image. As noted in section 2.3.3 the minimum average extent of a tree to be measured for analysis was 12 metres in order to ensure approximately 50% pixel coverage if the tree lies completely in one pixel. By analysing the data from the field, however, it was observed that though the average extent of the trees was approximately 13 metres, the majority of the trees recorded had minimum canopy extent ranging from 8 metres to 12.8 metres and maximum canopy extent ranging from 10.8 metres to 15.6 metres. The effect of the small canopy sizes recorded coupled with the fact that trees would not always be exactly in the middle of a pixel meant that the number of pixels that represent a tree canopy was, in most cases less than one (1). As a result many tree canopies were wholly or partially misclassified.

If the image resolution was finer, for example 5 metres as in RapidEye (RapidEye AG, 2012), then the number of pixels representing a tree canopy, even in extreme cases would be about four (4). This condition would have maximised the classification and object detection accuracies of both MLC and MRF-SRM techniques.

4.3.1 Effect of Crops on Tree Identification

It was observed that the intermingling of trees with crops (cocoa trees) did not have a direct impact on the tree canopy identification rate. This evidenced by the fact that the Maximum Likelihood Classifier, a pixel based classifier, correctly identified 34.88% of pixels as trees in spite of the limitations posed by tree canopy size to pixel size. This was markedly higher than the percentage of pixels misclassified as cocoa and could have been better but for the interference of the highly divergent Mixed Farms/Fallow class.

In the case of the MRF-SRM canopy identification, the results were not as high as expected. This was mostly due to the 'smoothing out' effect of the technique rather than one caused by the proximity of crops to trees.

4.4 Limitations

4.4.1 GPS Positional Accuracy

It was observed during the data collection that the positional accuracy of the GPS Receiver ranged from 20 metres to 50 metres when under a tree canopy. This large error could lead to tree identification errors during the canopy delineation stage. In view of this, whenever a tree's location was to be measured, a clearing of about four metre radius with an open view of the sky would be located. The GPS receiver was then placed on the ground in the clearing for three to five minutes within which time the positional accuracy would fall to 3 to 5 metres. A bearing and distance would then be taken from the location of the GPS receiver to the tree whose canopy was to be measured. For all subsequent trees within a 30 metre. Doing this ensured that the location of trees on the field could be correctly and easily located for delineation on the WorldView-2 image.

4.4.2 Effect of Season on Classification

The satellite images used were acquired in the months of January and February 2011 when cloud cover is low. These two months, however, fall in the dry season which lasts from November to March. Within this period, plants' access to water is fairly limited which leads to about 55% of thicket species and 19% of trees losing their leaves (Lieberman, 1982).

Since the research was carried out in the semi-deciduous zone, however, the observed leaf loss was not pronounced, especially in the trees and perennial crops. What was observed though was that, most probably due to the reduced availability of water, there was no leaf flush, as noted by Lieberman (1982) and Murphy and Lugo (1986). As a consequence, there was a reduced separability between the land cover classes identified which, as a result, influenced the accuracy of image classification using the Maximum Likelihood Classifier.

4.4.3 Effect of Spatial Resolution

Objects in real life cannot be adequately represented by pixels, irrespective of how fine they are (Fisher, 1997). Due to this fact, it is quite common that at all scales, attempts are made to extract information that is smaller than the size of a pixel. This pixel limitation was one that had to be dealt with in the study.

As it is technically impossible, especially considering the constraints of this study, to precisely identify the tree canopies and delineate them into a shape file, a pan-sharpened WorldView-2 image (0.5 metre resolution) was used as a base layer to obtain the closest representation of the measured tree canopy.

After the delineation of the tree canopies, it was observed that in the majority of cases, a tree would not completely cover one pixel on the ASTER image. Trees would, in most cases, straddle two or more pixels. Consequently, the identification rate of tree canopies in the MLC output image was negatively affected; isolated trees often got classified as the surrounding vegetation even though the tree canopy was larger than a pixel and would most likely have been classified as *Tree* if it had been positioned more appropriately (Figure 4.2).

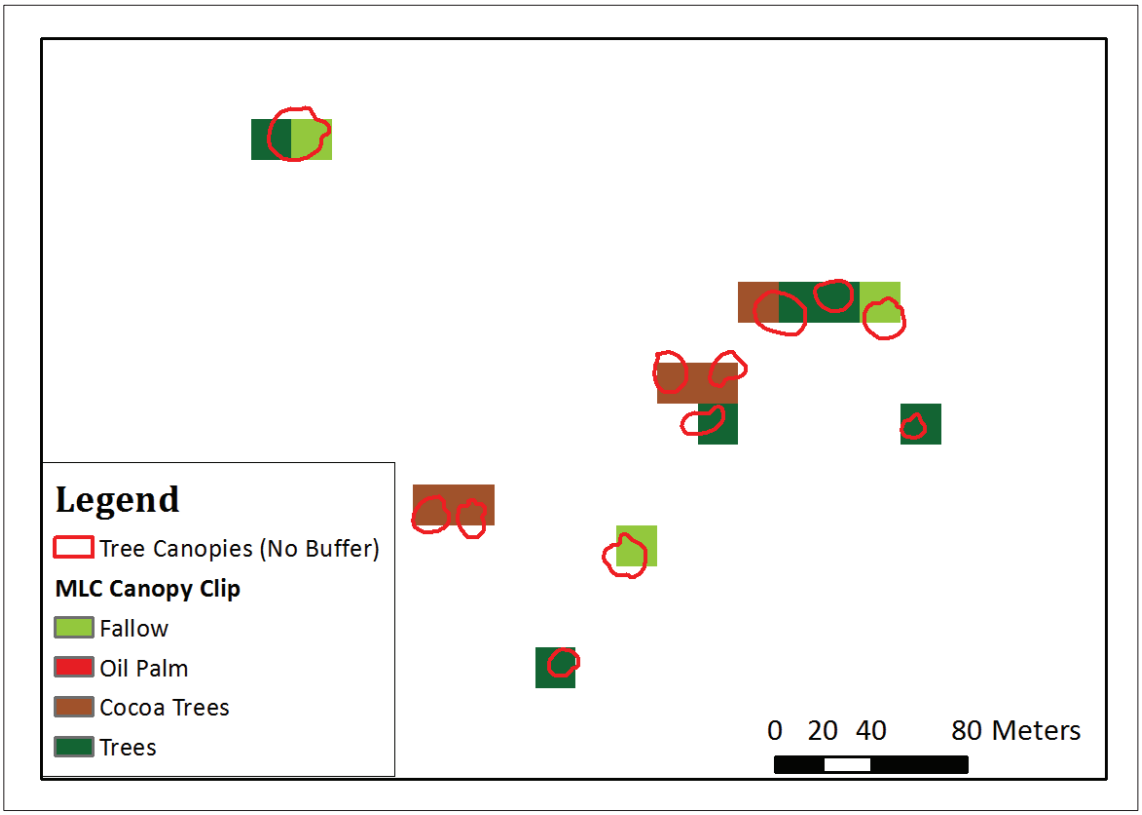

Figure 4.2: Subset of MLC Output showing effect of object positioning on pixel extraction

Another limitation of the spatial resolution of the images was observed during the extraction of the tree canopies. The coarse nature of the MLC output meant that a compromise had to be reached. Extraction of pixels using unbuffered tree canopies would result in a number of cases where trees that were measured on the field would not be extracted or in some cases extracted only partially.

The workaround for extracting the pixels covered by tree canopies was to buffer the canopies. After a series of trials with buffer sizes of 10% to 100% of the pixel size, it was observed that buffering by 25% of the image resolution extracted the pixels covered by tree canopies while keeping the amount of extracted background data to a minimum. This, therefore, was used as the guideline for buffering the tree canopy shape files which were then used to extract the tree canopies.

CHAPTER FIVE

5 CONCLUSIONS

5.1 Conclusions

This study compared the relative accuracy of mapping trees on farmlands using Markov Random Field Super-Resolution Mapping and Maximum Likelihood Classifier. In order to do this, the following research questions were addressed:

1. **Can SRM improve mapping trees on farmlands with reference to MLC?**

   Earlier studies have shown the ability of a variety of SRM techniques to produce better image classification results than pixel-based techniques like MLC. They did not state, however, how well SRM is able to identify individual objects in the image. This study shows that the Markov Random Field SRM technique does not improve mapping trees on farmlands as compared to the Maximum Likelihood Classifier since only 17.96% of tree canopies can be correctly identified using MRF-SRM while a much higher identification rate of 34.88% can be obtained using MLC.

2. **Does the presence or otherwise of farm crops affect the identification of trees using SRM?**

   There are two factors found that could make the presence of farm crops affect the identification of trees; size of object in relation to pixel size of input image and spectral separability of the input classes.

   The MRF-SRM technique used does a pixel-based pre-classification of the input image before performing the resolution enhancement. If, therefore, the size of the feature one wants to identify do not occupy the majority of a pixel, then the feature will not be correctly classified in the initial classification and subsequently it will not appear in the resolution-enhanced image. In the case of identification of trees on farmlands, the presence of farm crops do not directly affect the identification of trees, except when the majority of the pixel is covered by farm crops.

   It was also observed that if the band separability between the crop class(es) and tree classes is poor, as is usually the case during the dry season, then the presence of crops will affect the identification of trees.

REFERENCES

Abrams, Mi., & Hook, S. (n.d.). ASTER User's Handbook v2. Jet Propulsion Laboratory. Retrieved from http://asterweb.jpl.nasa.gov/content/03_data/04_Documents/aster_user_guide_v2.pdf

Anornu, G. K., Kortatsi, B. K., & Saeed, Z. M. (2010). Evaluation of groundwater resources potential in the Ejisu-Juaben district of Ghana. *African Journal of Environmental Science and Technology*, *3*(10). doi:10.4314/ajest.v3i10.56261

Ardila, J. P., Tolpekin, V. A., Bijker, W., & Stein, A. (2011). Markov-random-field-based super-resolution mapping for identification of urban trees in VHR images. *ISPRS Journal of Photogrammetry and Remote Sensing*, *66*(6), 762–775. doi:10.1016/j.isprsjprs.2011.08.002

Atkinson, P. M. (2008). Super-Resolution Mapping Using the Two-Point Histogram and Multi-Source Imagery. In A. Soares, M. J. Pereira, & R. Dimitrakopoulos (Eds.), *geoENV VI – Geostatistics for Environmental Applications* (Vol. 15, pp. 307–321). Springer Netherlands. Retrieved from http://www.springerlink.com/content/l023534665535822/abstract/

Atkinson, Peter M. (2004). Resolution Manipulation and Sub-Pixel Mapping. In S. M. D. Jong & F. D. V. der Meer (Eds.), *Remote Sensing Image Analysis: Including The Spatial Domain* (pp. 51–70). Springer Netherlands. Retrieved from http://link.springer.com/chapter/10.1007/978-1-4020-2560-0_4

Dial, G., & Grodecki, J. (2003). Applications of IKONOS imagery. In *American Society for Photogrammetry and Remote Sensing 2003 Annual Conference, Anchorage, Alaska. Proceedings*. Retrieved from http://geoeye.com/CorpSite/assets/docs/technical-papers/2003/B_DialGene_JacekGrodecki_2003_2.pdf

Dumanski, J. (2004). Carbon Sequestration, Soil Conservation, and the Kyoto Protocol: Summary of Implications. *Climatic Change*, *65*(3), 255–261. doi:10.1023/B:CLIM.0000038210.66057.61

FAO. (2006, March 27). Forests and climate change. Retrieved 30 May 2012, from http://www.fao.org/newsroom/en/focus/2006/1000247/index.html

FAO. (2010). *Global Forest Resources Assessment 2010*. Rome. Retrieved from http://www.fao.org/docrep/013/i1757e/i1757e.pdf

FAO. (2011, November 30). Global forest land-use change from 1990 to 2005: Initial results from a global remote sensing survey. FAO. Retrieved from http://foris.fao.org/static/data/fra2010/RSS_Summary_Report_lowres.pdf

Fisher, P. (1997). The pixel: A snare and a delusion. *International Journal of Remote Sensing*, *18*(3), 679–685. doi:10.1080/014311697219015

Gibbs, H. K., Brown, S., Niles, J. O., & Foley, J. A. (2007). Monitoring and estimating tropical forest carbon stocks: making REDD a reality. *Environmental Research Letters*, *2*(4), 045023. doi:10.1088/1748-9326/2/4/045023

Kasetkasem, T., Arora, M. K., & Varshney, P. K. (2005). Super-resolution land cover mapping using a Markov random field based approach. *Remote Sensing of Environment*, *96*(3–4), 302–314. doi:10.1016/j.rse.2005.02.006

Li, S. Z. (2009). *Markov random field modeling in image analysis* (Third.). Springer London. Retrieved from http://www.springerlink.com/book/10.1007/978-1-84800-279-1/page/1

Lieberman, D. (1982). Seasonality and Phenology in a Dry Tropical Forest in Ghana. *Journal of Ecology*, *70*(3), 791–806. doi:10.2307/2260105

Merino, M. T., & Nunez, J. (2007). Super-Resolution of Remotely Sensed Images With Variable-Pixel Linear Reconstruction. *Geoscience and Remote Sensing, IEEE Transactions on*, *45*(5), 1446 –1457. doi:10.1109/TGRS.2007.893271

Ministry of Food & Agriculture, Ghana. (2011). Ejisu-Juaben. *Ministry of Food & Agriculture*. Retrieved 22 August 2012, from http://mofa.gov.gh/site/?page_id=855

Muad, A. M., & Foody, G. M. (2010). Super-Resolution Mapping of Landscape Objects from Coarse Spatial Resolution Imagery. In E.A. Addink & F.M.B. Van Coillie (Eds.), (Vol. XXXVIII–4/C7, 2010, p. 6). Presented at the GEOBIA 2010: Geographic Object-Based Image Analysis, Ghent, Belgium. Retrieved from http://www.isprs.org/proceedings/XXXVIII/4-C7/pdf/Muad_100.pdf

Murphy, P. G., & Lugo, A. E. (1986). Ecology of Tropical Dry Forest. *Annual Review of Ecology and Systematics*, *17*, 67–88. doi:10.2307/2096989

Padwick, C., Deskevich, M., Pacifici, F., & Smallwood, S. (2010). WorldView-2 pan-sharpening. In *American Society for Photogrammetry and Remote Sensing*.

Parker, C., Mitchell, A., Trivedi, M., & Mardas, N. (2009). *The Little REDD+ Book* (3rd ed.). Oxford, UK: Global Canopy Programme. Retrieved from http://www.theredddesk.org/sites/default/files/lrb_en.pdf

R Core Team. (2012). *R: A Language and Environment for Statistical Computing*. Vienna, Austria: R Foundation for Statistical Computing. Retrieved from http://www.r-project.org

RapidEye AG. (2012, January). RapidEye Product Specifications. Retrieved from http://www.rapideye.net/upload/RE_Product_Specifications_ENG.pdf

RStudio: Integrated development environment for R. (2012). Boston, MA: RStudio. Retrieved from http://www.rstudio.org

Satellite Imaging Corporation. (n.d.). WorldView-2 Satellite Sensor Information and Specifications. Retrieved 12 February 2013, from http://www.satimagingcorp.com/satellite-sensors/worldview-2.html

Schowengerdt, R. A. (2006). *Remote sensing, models, and methods for image processing* (3rd ed.). San Diego, California: Academic Press. Retrieved from http://www.dawsonera.com/depp/reader/protected/external/AbstractView/S9780080480589/S8.71/0

Stewart, J. (n.d.). *SciA: 17 Jan 13: Crabs feel pain*. Retrieved from http://downloads.bbc.co.uk/podcasts/worldservice/scia/scia_20130117-2032a.mp3

Tatem, A. J., Lewis, H. G., Atkinson, P. M., & Nixon, M. S. (2001). Super-resolution target identification from remotely sensed images using a Hopfield neural network. *Geoscience and Remote Sensing, IEEE Transactions on*, *39*(4), 781 –796. doi:10.1109/36.917895

Tatem, A. J., Lewis, H. G., Atkinson, P. M., & Nixon, M. S. (2003). Increasing the spatial resolution of agricultural land cover maps using a Hopfield neural network. *International Journal of Geographical Information Science*, *17*(7), 647–672. doi:10.1080/1365881031000135519

Tolpekin, V. A., Ardila, J. P., & Bijker, W. (2010). Super-resolution mapping for extraction of urban tree crown objects from VHR satellite images. In E.A. Addink & F.M.B. Van Coillie (Eds.), (Vol.

XXXVIII–4/C7, 2010, p. 7). Presented at the GEOBIA 2010: Geographic Object Based Image Analysis, Ghent, Belgium.

Tong, X., Zhang, X., Shan, J., Xie, H., & Liu, M. (2012). Attraction-Repulsion Model-Based Subpixel Mapping of Multi-/Hyperspectral Imagery. *IEEE Transactions on Geoscience and Remote Sensing*, *PP*(99), 1 –16. doi:10.1109/TGRS.2012.2218612

Weiss, N. A. (2012). *Introductory statistics*. Boston: Pearson Addison-Wesley.

APPENDICES

APPENDIX I: Bootstrapping Code For Test of Significance

```
/*
 * Title:       Accuracy assessment bootstrapper
 * Author:      Franz Alex Gaisie-Essilfie
 * Date:        March 11, 2013
 * Language:    Visual C#
 * Requirement: .NET 3.5 or higher
 * Disclaimer:  This code was developed by Franz Alex Gaisie-Essilfie for the sole
 *              purpose of bootstrapping samples obtained from an accuracy
 *              assessment data.
 *              It is allowed to use this code for research purpose only.
 *              The code is distributed "as is", WITH NO WARRANTY whatsover.
 *              The author does not guarantee its suitability for any purpose
 *              other than what it was designed for.
 */
using System;
using System.Collections.Generic;
using System.Linq;

namespace AccuracyReplicator
{
    class Program
    {
        static void Main(string[] args)
        {
            Console.WriteLine("Enter the path to the CSV Data file");
            var fileName = Console.ReadLine().Trim('"').Trim();

            // ensure the file exists.
            if (!System.IO.File.Exists(fileName))
            {
                Console.Write("The specified file does not exist.\r\n" +
                              "Press ENTER to exit.");
                Console.ReadLine();
                return;
            }

            var fileData = ReadFile(fileName).ToList();
            var fileFields = fileData[0];
            fileData = fileData.Skip(1).ToList();
            var dataCount = fileData.Count;

            // file info
            Console.WriteLine();
            Console.WriteLine("Number of Records: " + fileData.Count.ToString());
            Console.WriteLine("Fields: " + string.Join("; ", fileFields));
            Console.WriteLine();

            // ask for columns
            Console.WriteLine("Enter the fields you want to replicate " +
                              "in the format \r\n" + "RealValue; Observed1" +
                              "[; Observed2][; Observed3][...]");
            var workingFields = from p in Console.ReadLine().Trim().Split(';')
                                select p.Trim();

            // ask for replicate info
            Console.Write("Enter the number of records per sample: ");
            var sampleSize = Math.Min(Convert.ToInt32(Console.ReadLine().Trim()),
```

```
                                dataCount);
            Console.Write("Enter the number of times to replicate: ");
            var replicates = Math.Min(Convert.ToDouble(Console.ReadLine().Trim()),
                                dataCount);

            var fieldIdx = (from f in workingFields
                            where fileFields.Contains(f)
                            select fileFields.ToList().IndexOf(f)).ToArray();

            var results = new List<double[]>();


            // bootstrap replicates of the data
            while (results.Count < replicates)
            {
                var values = Randomize(fileData).Take(sampleSize).ToArray();
                var result = new List<double>();
                var trueIdx = fieldIdx[0];
                foreach (int idx in fieldIdx.Skip(1))
                {
                    var trueCount = 0.0;
                    foreach (var rec in values)
                        if (rec[trueIdx] == rec[idx])
                            trueCount += 1;

                    result.Add(trueCount / sampleSize);
                }

                results.Add(result.ToArray());
            }


            // write the result
            var outFile = fileName.Substring(0, fileName.LastIndexOf('.')) +
                          " - Replicate.csv";
            using (var sw = new System.IO.StreamWriter(outFile))
            {
                sw.Write("Replicate");
                foreach (var i in fieldIdx.Skip(1))
                    sw.Write("," + fileFields[i]);
                sw.WriteLine();

                for (int i = 0; i < results.Count; i++)
                {
                    sw.Write((i + 1).ToString() + ",");
                    sw.WriteLine(string.Join(",", results[i].
                                        Select(x => x.ToString()).ToArray())
                                );
                }
            }

            // open the file
            System.Diagnostics.Process.Start(outFile);

            Console.ReadLine();
        }

        static IEnumerable<string[]> ReadFile(string fileName)
        {
            /*
             * Rudimentary CSV file reader.
             * Not guaranteed to read all CSV files;
             * especially when fields contain spaces.
             */
            using (var sr = new System.IO.StreamReader(fileName))
```

```
                while (!sr.EndOfStream)
                    yield return (from p in sr.ReadLine().TrimEnd().Split(',')
                                  select p.Trim()).ToArray();
        }

        static double Combinations(int n, int k)
        {
            // factorials of the inputs.
            // n! has (n-k)! removed to simplify calculations
            // Decimal is used to reduce floating point rounding errors
            var kFact = Enumerable.Range(1, k).Select(i => Convert.ToDecimal(i)
                                                    ).ToArray();
            var n_kFact = Enumerable.Range(1, n - k)
                                    .Select(i => Convert.ToDecimal(i)).ToArray();
            var nFact = Enumerable.Range(1, n).Select(i => Convert.ToDecimal(i)
                                                    ).Except(n_kFact).ToArray();

            // ensure there is something to process
            if (!kFact.Any()) kFact = new decimal[] { 1 };
            if (!nFact.Any()) nFact = new decimal[] { 1 };

            // good old division by cancellation
            for (int i = 0; i < Math.Min(kFact.Count(), nFact.Count()); i++)
            {
                nFact[i] /= kFact[i];
                kFact[i] = 1;
            }

            // multiply the numerators and the denominators
            // then divide both products
            return Convert.ToDouble(nFact.Aggregate((x, y) => x * y) /
                                    kFact.Aggregate((x, y) => x * y));
        }

        static Random rnd = new Random();
        static IEnumerable<T> Randomize<T>(IList<T> set)
        {
            var nums = Enumerable.Range(0, set.Count - 1).ToArray();

            for (int i = nums.Length; i > 1; i--)
            {
                // Pick random element to swap.
                int j = rnd.Next(i); // 0 <= j <= i-1
                // Swap.
                var tmp = nums[j];
                nums[j] = nums[i - 1];
                nums[i - 1] = tmp;
            }


            // use the shuffled numbers to return random elements in the set
            foreach (int i in nums)
                yield return set[i];
        }
    }
}
```